

RELIABILITY-BASED SEISMIC DEFORMATION ANALYSIS OF REINFORCED SOIL SLOPES

MASAHIRO SHINODAⁱ⁾, KATSUMI HORIIⁱⁱ⁾, TOYOJI YONEZAWAⁱⁱⁱ⁾, MASARU TATEYAMA^{iv)} and JUNICHI KOSEKI^{v)}

ABSTRACT

The paper describes a precise technique to compute the limit state exceedance probability of typical earth slopes and geosynthetic-reinforced soil (GRS) slopes using a low-discrepancy sequence Monte Carlo (LDSMC) method and an importance sampling with low-discrepancy sequence Monte Carlo (ISLDSMC) method. The LDSMC and ISLDSMC methods can efficiently compute the accurate limit state exceedance probabilities of typical earth slopes and GRS slopes with a limited number of simulations. This study presents a practically useful nomogram of seismic deformation and limit state exceedance probability with variable slope heights, backfill soil properties, and geometries. A simple estimation of the limit state exceedance probability of the GRS slopes is given based on the results of the conventional deterministic analysis. The results of these analyses show that the LDSMC and ISLDSMC methods are practically useful, efficient, and accurate for the limit state exceedance probability calculation.

Key words: deformation analysis, earthfill, low-discrepancy sequence, quasi-Monte Carlo simulation, reinforced soil slope, stability analysis (IGC: E2/E6/E13)

INTRODUCTION

The conventional deterministic method using a safety factor can partially consider the variability of soil properties when the design values are selected with a certain confidence while taking into account the average and standard deviation of input soil parameters. This method, however, cannot quantitatively evaluate the failure probability. To overcome such a problem, in recent years, civil engineers have focused on a reliability analysis based on the probability theory. One advantage of working with reliability analysis is that the variability of soil parameters can be considered rationally and quantitatively by using a reliability index, failure probability, or limit state exceedance probability. Another advantage of this analysis is that the reliability can be used in an economic cost-benefit analysis that takes into account the design and construction costs as well as the implications of design failure. Although the advantages of reliability analysis are generally acknowledged at present, there are only a limited number of applications for dealing with the practical problems of embankments (Matsuo and Kuroda, 1974; Christian et al., 1994), earth slopes (Wu and Kraft, 1970; Alonso, 1976; Tang et al., 1976; Vanmarcke, 1977; Bergado,

1985; Li and Lumb, 1987; Duncan, 2000), retaining walls (Duncan, 2000; Hoeg and Murarka, 1974), and mechanically stabilized earth (MSE) walls (Low and Tang, 1997; Chalermyanont and Benson, 2004; Shinoda et al., 2005). Research on the design of geosynthetic-reinforced soil (GRS) slopes has been limited.

The algorithms to compute the reliability index or failure probability can be generally grouped into two categories, namely, approximate methods such as first-order reliability method (FORM) presented by Hasofer and Lind (1974) and simulation methods such as Monte Carlo simulation (e.g. El-Ramly et al., 2002; Lian and Yen, 2003). The approximate methods present a practical approach to enumerate significant failure sequences, while they involve restrictive simplifying assumptions on structural behavior and approximate bounds during probability computation. When these methods are applied to a complex problem, an impermissible computational error might be induced. On the other hand, the simulation methods are easier to implement, robust in performance, and can incorporate a realistic structural behavior; however, they tend to be computationally expensive for high-reliability structures. Therefore, some improvement in the latter methods is needed in order to reduce the computational time.

ⁱ⁾ Doctor of Engineering, Integrated Geotechnology Institute, Engineering Department, Japan (shinoda@igi.co.jp).

ⁱⁱ⁾ Integrated Geotechnology Institute, Engineering Department, Japan (horii@igi.co.jp).

ⁱⁱⁱ⁾ Japan Railway Construction, Transport and Technology Agency, Japan (t.yonezawa@jrtr.go.jp).

^{iv)} Doctor of Engineering, Railway Technical Research Institute, Foundation and Geotechnical Engineering Structures Technology Division, Japan (tate@rtri.of.jp).

^{v)} Doctor of Engineering, University of Tokyo, Institute of Industrial Science, Japan (koseki@iis.u-tokyo.ac.jp).

The manuscript for this paper was received for review on September 21, 2005; approved on March 10, 2006.

Written discussions on this paper should be submitted before March 1, 2007 to the Japanese Geotechnical Society, 4-38-2, Sengoku, Bunkyo-ku, Tokyo 112-0011, Japan. Upon request the closing date may be extended one month.

This study deals with an application of the reliability analysis in order to investigate the structural reliability of typical GRS slopes—subjected to strong earthquakes—with variable heights, backfill soil properties, and geometries by the advanced Monte Carlo techniques. In evaluating their stability, the Railway Technical Research Institute (RTRI) design code (RTRI, 2000) was employed in this analysis.

OBJECTIVE OF ANALYSIS

The principal objective of the current reliability analysis described in this study is to investigate the effects of soil properties, slope height, and structural level on the earthquake-induced residual deformation (herein called as seismic deformation) and limit state exceedance probability of typical earth slopes (without reinforcement) and GRS slopes. This paper presents two types of nomograms. One is the seismic deformations of earth slopes and GRS slopes subjected to a design ground motion by a deterministic seismic deformation analysis. The other is the limit state exceedance probability of earth slopes and GRS slopes subjected to the same load condition by a probabilistic seismic deformation analysis. In order to simplify the calculation of the limit state exceedance probability of the GRS slopes, a simple estimation of the limit state exceedance probability was presented. A feature of the current analysis is a precise reliability analysis technique to compute a wide range of limit state exceedance probabilities using the Monte Carlo method with a low-discrepancy sequence that is less time consuming.

METHOD FOR DETERMINISTIC AND PROBABLISTIC ANALYSES

Newmark's Sliding Block Analysis

In the current study, Newmark's sliding block analysis (Newmark, 1965) was adopted for the seismic deformation analysis. It is a simplified procedure employed in the design code of railway structures in Japan (RTRI, 2000), in which the seismic deformation of earth slopes or GRS slopes subjected to a strong ground motion can be calculated by integrating the equation of rotational motion of a soil mass contained within the critical circular slip surface by assuming the failure mass as a rotational rigid block. The equation of rotational motion is solved for the rotation caused by the difference between the driving and resisting moments. The critical slip surface is determined by the conventional modified Fellenius method (Fellenius, 1927) using a specific acceleration or seismic coefficient to yield a safety factor of 1.0. Hereafter, this acceleration and seismic coefficient will be referred to as the yield acceleration and yield seismic coefficient, respectively. A requisite for such an analysis is the unit weight, friction angle and cohesion of soil, and design strength of reinforcement. For calculating seismic deformation, it is not necessary to consider input parameters in addition to the abovementioned ones. The

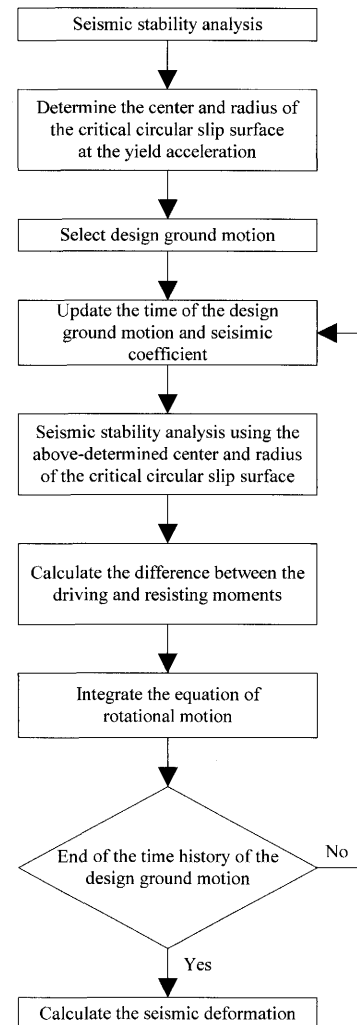


Fig. 1. Flow chart of the standard Newmark analysis employed in the RTRI design code (2000)

feature of this analysis is that it is practically useful and less time consuming in terms of calculation. Newmark's sliding block analysis will be hereafter referred to as Newmark analysis.

Figure 1 shows the flow chart of the standard deterministic Newmark analysis according to the RTRI design code. The seismic stability analysis is conducted with the conventional modified Fellenius method to determine the center and radius of the critical circular slip surface and yield acceleration. The safety factor in the above seismic stability analysis can be obtained from the following equation:

$$FS = \frac{M_r}{M_d} = \frac{M_{rw} + M_{rc} + M_{rt} - k_h M_{rk}}{M_{dw} + k_h M_{dk}} \quad (1)$$

where FS is the safety factor; k_h , seismic coefficient; M_r , overall resisting moment; M_d , overall driving moment; M_{rw} , resisting moment due to the self-weight of soil; M_{rc} , resisting moment due to soil cohesion; M_{rt} , resisting moment due to the design strength of reinforcement; M_{rk} , decrease in the resisting moment per unit seismic coefficient due to the self-weight of soil subjected to a

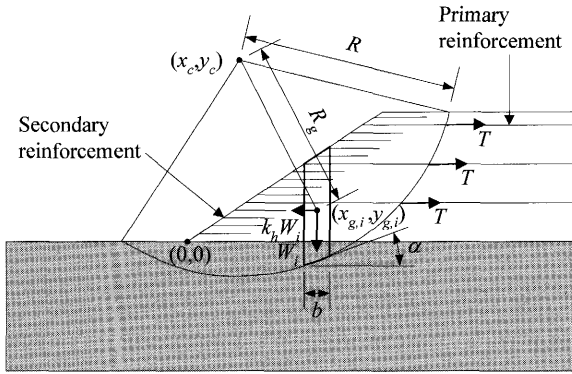


Fig. 2. Notations of the geosynthetic-reinforced soil (GRS) slope

seismic inertia force; M_{dw} , driving moment due to the self-weight of soil; and M_{dk} , driving moment per unit seismic coefficient due to the seismic inertia force. By substituting $FS=1.0$ and arranging Eq. (1), the yield seismic coefficient is obtained as follows:

$$k_y = \frac{M_{rw} + M_{rc} + M_{rt} - M_{dw}}{M_{dk} + M_{rk}} \quad (2)$$

Each component of Eq. (1) and Eq. (2) can be calculated as follows:

$$M_{rw} = R \sum (W_i \cdot \cos \alpha_i \cdot \tan \phi) \quad (3)$$

$$M_{rc} = R \sum (c \cdot l_i) \quad (4)$$

$$M_{rt} = R \sum \{T_i \cdot (\sin \alpha_i \cdot \tan \phi + \cos \alpha_i)\} \quad (5)$$

$$M_{rk} = R \sum (W_i \cdot \sin \alpha_i \cdot \tan \phi) \quad (6)$$

$$M_{dw} = \sum \{(x_{g,i} - x_c) \cdot W_i\} \quad (7)$$

$$M_{dk} = \sum \{(y_c - y_{g,i}) \cdot W_i\} \quad (8)$$

The notations are defined in Fig. 2, where R is the radius of the critical circular slip surface; W_i , soil weight of the i -th slice; α_i , angle between the critical slip surface and x coordinate of the i -th slice; ϕ , soil friction angle; c , soil cohesion; l_i , length of the critical slip surface of the i -th slice; $x_{g,i}$ and $y_{g,i}$, the x and y coordinates of the center of gravity of the i -th slice, respectively; and x_c and y_c , the x and y coordinates of the center of the critical slip surface, respectively. T_i is the design strength of the reinforcement of the i -th slice, which is obtained as follows:

$$T = \min \{T_a, T_p\} \quad (9)$$

where T_a is the allowable tension load obtained from the standard extension tests according to the RTRI design code, which is obtained as follows:

$$T_a = RF \cdot T_w \quad (10)$$

where T_w is the warranted tensile strength specified by a manufacturer, and RF is the product of all applicable reduction factors. The time-dependent strength losses due to creep or relaxation are not considered according to the RTRI seismic design code; which is consistent with

the findings of Bernardi and Paulson (1997), Orsat et al. (1998), Greenwood et al. (1997, 2000, 2001), Voskamp et al. (2001), and Shinoda et al. (2002). T_p in Eq. (9) is the resisting force against the pullout of the reinforcement according to the RTRI design code, which is obtained as follows:

$$T_p = \frac{2.0 \cdot L_i \cdot \sigma_v \cdot \tan \phi}{F_f} \quad (11)$$

where L_i is the reinforcement length in the outside of the critical slip surface; σ_v is the vertical stress on the i -th reinforcement; and F_f is the safety factor.

Each value is defined as the load per unit width of the reinforcing basis. For example, it is assumed that the reinforcement has 20 longitudinal members per meter and the tension load of the reinforcement with 4 longitudinal members is 18 kN in the standard extension tests. The load per unit width of the reinforcing basis is 18 kN multiplied by the ratio of the number of longitudinal members in the test per meter, that is, the product is 90 kN/m.

Subsequently, after selecting the design ground motion, the seismic stability analysis is conducted by using the above-determined center and radius of the critical slip surface. The seismic coefficient is updated as follows:

$$k_h(t) = \frac{A(t)}{g} \quad (12)$$

where $A(t)$ is the acceleration time history of the design ground motion, and g is the gravitational acceleration.

The above seismic stability analysis is performed up to the end of the time history of design ground acceleration. During the seismic stability analysis, the difference between the overall driving and resisting moments is calculated, and the equation of rotational motion is obtained as follows:

$$J\ddot{\theta}(t) = M_d(t) - M_r(t) \\ = M_{dw} + k_h M_{dk} - M_{rw} + k_h M_{rk} - M_{rc} - M_{rt} \quad (13)$$

where θ is the rotational angle of the soil mass and J is the moment of inertia expressed as follows:

$$J = \sum \left(J_{g,i} + \frac{1}{g} \cdot R_{g,i}^2 \cdot W_i \right) \quad (14)$$

where $J_{g,i}$ is the polar moment of inertia of the i -th slice and $R_{g,i}$ is the distance between the center of the slice and that of the critical circular slip surface of the i -th slice, as shown in Fig. 2. The angular acceleration, angular velocity, and rotation of the soil mass are obtained as follows:

$$\ddot{\theta}_{t+\Delta t} = \frac{1}{J} \Delta M_{t+\Delta t} \quad (15)$$

$$\dot{\theta}_{t+\Delta t} = \dot{\theta}_t + \frac{1}{2} \cdot (\ddot{\theta}_t + \ddot{\theta}_{t+\Delta t}) \cdot \Delta t \quad (16)$$

$$\theta_{t+\Delta t} = \theta_t + \dot{\theta}_t \cdot \Delta t + \frac{1}{6} \cdot (2 \cdot \ddot{\theta}_t + \ddot{\theta}_{t+\Delta t}) \cdot \Delta t^2 \quad (17)$$

The accumulated rotation of the soil mass is computed

using Eq. (17) only when the angular velocity is positive. Finally, the seismic deformation is obtained as follows:

$$d_t = R \cdot \theta_t \quad (18)$$

In this paper, the seismic deformation is defined as a rotational displacement along the critical slip surface of the failure mass according to the RTRI design code.

Quasi Monte Carlo Simulation

In reliability analyses, the reliability of a structure can be evaluated by the sign of the performance function. For example, a reliable or safe structure has a positive performance function, while an unreliable or unsafe structure that exceeds the limit state has a zero or negative performance function. In this study, the following performance function was employed for the reliability evaluation:

$$Z = 1.0 - \frac{D}{D_L} \quad (19)$$

where Z is the performance function; D , the seismic deformation calculated by the Newmark analysis; and D_L , the allowable seismic deformation (i.e., upper bound of seismic deformation). This allowable seismic deformation is determined by engineers, considering the importance of a structure or its lifetime. In the present study, D_L was assumed to be 50 cm; this was considered to be the critical seismic deformation for the earth slopes or GRS slopes considered by the authors. Hereafter, this allowable seismic deformation will be referred to as the critical seismic deformation. The seismic deformation calculation is repeated with variable input parameters up to the prescribed number of simulations. The limit state exceedance probability is then obtained as follows:

$$P_1 = \frac{N_{Z \leq 0}}{N} \quad (20)$$

where P_1 is the limit state exceedance probability; N , the total number of simulations, and $N_{Z \leq 0}$, the number that corresponds to the case in which the performance function has zero or negative values. The corresponding reliability index is calculated as follows:

$$\beta = \Phi^{-1}(P_1) \quad (21)$$

where β is the reliability index, and Φ^{-1} is the inverse function of the standard normal probability distribution function.

The above described solution is known as crude Monte Carlo (CMC) simulation. In general, the CMC simulation tends to be computationally expensive for calculating the limit state exceedance probability. There are two practical problems in this simulation: One is the non-uniformity of input parameters and the other is the dependency of the simulation result on the number of simulations. The first problem is caused by random input parameters generated by the classical or conventional random sampling scheme, which is a non-uniformity distribution under a small number of simulations, inducing an impermissible numerical error. Figure 3(a) shows a

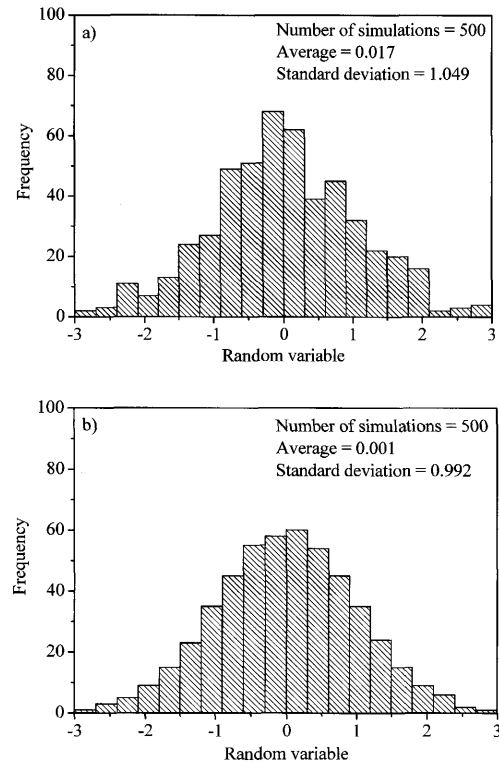


Fig. 3. Histogram of a random variable with standard normal distribution: a) Conventional Box-Muller method and b) Low-discrepancy sequence

typical histogram of a normally distributed random variable assuming an average of 0.0 and standard deviation of 1.0 (standard normal distribution) obtained by using the conventional random generator (Box and Muller, 1958) with 500 simulations. It is evident that the random variable was not uniform when the average and standard deviation could not be achieved with the prescribed values. Moreover, the above random variable strongly depends on the seed, which means that the above random variable is not unique with the various seeds for a small number of simulations, inducing a numerical error. To reduce such numerical errors, a low-discrepancy sequence (LDS) was adopted in the proposed Monte Carlo simulation referred to as LDSMC. The LDS is one of the quasi-random numbers having a uniform distribution (i.e., Tezuka, 1995). A feature of the LDS is that a set of quasi-random numbers in each simulation is unique with respect to the number of simulations. Figure 3(b) shows the histogram of the standard normal distribution using the LDS under the same numerical condition, as shown in Fig. 3(a). The uniformity of the random variable could be significantly improved by using the LDS. A detailed process to generate the LDS is explained in the Appendix. Based on the above results, it is fairly reasonable to use the LDS for random numbers in the current Monte Carlo simulation.

The second problem is that the requisite for the order of the limit state exceedance probability to range from 10^{-2} to 10^{-5} is an incredibly large number of simulations ranging from 1,000 to 1,000,000. However, if random

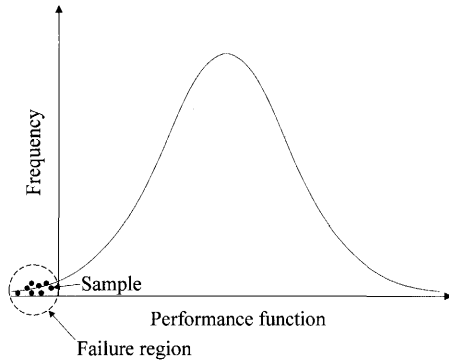


Fig. 4. Failure region of a typical normal probability density function of performance function

variables can be generated in the expected failure region (i.e., the tail of the statistical distribution of the performance function, as shown in Fig. 4), it is easy to enumerate the number of failures by the Monte Carlo simulation. This sampling scheme is termed importance sampling (IS). The limit state exceedance probability of the structures by the importance sampling Monte Carlo simulation (ISMC) is calculated by using the following equation:

$$P_1 = \int \cdots \int I[Z(x) \leq 0] \cdot h_v(x) \cdot \frac{f_x(x)}{h_v(x)} dx \quad (22)$$

where $I[x]$ is the Heaviside step function. In this function, if x is true, $I=1$, and if x is false, $I=0$. $f_x(x)$ is a joint probability density function obtained by multiplying each probability density function. $h_v(x)$ is an IS density function. The IS density function used in this study is a joint probability density function. Each average of the IS density function corresponds to the design point obtained from the FORM (Hasofer and Lind, 1974), while each standard deviation of the IS density function corresponds to the standard deviation of the input random variables. Refer to Hasofer and Lind (1974) for a theoretical explanation of the FORM.

For example, to calculate limit state exceedance probability P_1 with normally distributed n random variables $\mathbf{x} = (x_1, x_2, \dots, x_n)^T$, $N_{Z \leq 0}$ in Eq. (20) is obtained by using the following equation:

$$N_{Z \leq 0} =$$

$$\sum_{j=1}^N \left[I[Z \leq 0] \cdot \prod_{i=1}^n \frac{\frac{1}{\sqrt{2\pi}\sigma_{x_i}} \exp \left\{ -\frac{1}{2} \left(\frac{x_i - \mu_{x_i}}{\sigma_{x_i}} \right)^2 \right\}}{\frac{1}{\sqrt{2\pi}\sigma_{x_i}} \exp \left\{ -\frac{1}{2} \left(\frac{x_i - \mu_{x_i}^*}{\sigma_{x_i}} \right)^2 \right\}} \right] \quad (23)$$

where μ_x and σ_x are the average and standard deviation of x ; μ_{x^*} is the average of x^* ; and x^* is the design point obtained from the FORM.

The advantage of the IS scheme is that the limit state exceedance probability can be calculated with a less number of simulations, resulting in lower computation time. The most effective method to compute the limit state

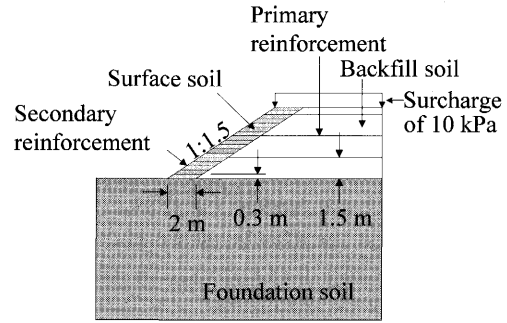


Fig. 5. Model description of the GRS slope

exceedance probability by using Eq. (20) is to generate random variables by the LDS around the expected failure region obtained from the result of the FORM shown in Fig. 4; this is termed "importance sampling with low-discrepancy sequence Monte Carlo (ISLDSMC) method" in this study.

ANALYTICAL MODEL AND INPUT PARAMETERS

Figure 5 shows the analytical model of a typical GRS slope. The slope inclination had a constant vertical to horizontal ratio of 1:1.5. The vertical spacings of the primary and secondary reinforcements were 1.5 m and 0.3 m, respectively. The length of the primary reinforcement was sufficiently long beyond the critical slip surface to resist the rotation of the soil mass, while the length of the secondary reinforcement was set constant at 2.0 m. A surcharge of 10 kPa was applied on the crest of the slope.

According to the RTRI design code, the properties of foundation soil, backfill soil, and surface soil need to be determined in order to evaluate the safety or reliability of a structure. In the current analysis, the foundation soil was assumed to have sufficiently high strength and stiffness. On the other hand, in practice, the surface soil along a slope is generally very difficult to compact, thus requiring a lower friction angle. Moreover, the cohesion of unsaturated surface soil generally depends on the degree of saturation. The degree of saturation of surface soil is usually higher due to the effects of rainfall. This indicates that the cohesion of surface soil may become lower than that of backfill soil. Thus, the properties of surface soil were modeled by using a relatively lower friction angle and cohesion than backfill soil. The design soil properties will be explained in the subsequent sections.

Figure 6 shows the geometries of all the models used in this analysis, categorized by the structural levels and slope heights. Level 1 geometry has primary and secondary reinforcements, as mentioned earlier. This GRS slope can be expected to have a high seismic stability. Level 2 geometry only has secondary reinforcements; thus, lower seismic stability is expected. Level 3 geometry has no reinforcement; this is referred to as earth slope in this study, and a much lower seismic stability is expected.

Figure 7 shows one of the standard design ground

motions specified in the design code of railway structures in Japan (RTRI, 2000). This design ground motion corresponds to a strong earthquake with the maximum acceleration of 924 gal. This standard design ground motion was used in the current analysis.

Table 1 shows the statistical soil properties referred by Watanabe et al. (2005); these are categorized into three groups according to the RTRI design code. As mentioned earlier, each soil group has two soil types: surface soil and backfill soil. The foundation soil properties were assumed to have a high internal friction angle and high cohesion so that the critical slip surface does not cross it. For the deterministic Newmark analysis, the average values of soil properties were used. Table 2 shows the reinforcement property in a statistical manner. In this study, due to the lack of statistical data on the extension tests of reinforcement, the coefficient of variation (COV) of the warranted tensile strength of the reinforcements was assumed to be 10%, which is equivalent to the COVs of

the internal friction angle and cohesion of soils. In the current analysis, the reduction factor to calculate the allowable tension load is set at a constant of 0.9 by only considering the effects of seismic loading, installation damage, and durability. The total number of random variables including the surface and backfill soil properties (density, friction angle, and cohesion) and the design strengths of primary and secondary reinforcements was eight. Each random variable was assumed to be statistically independent and normally distributed.

Verification of Proposed Quasi-Monte Carlo Method

The proposed quasi-Monte Carlo methods (LDSMC and ISLDSMC) were verified by comparing the results from the conventional CMC method with varying number of simulations. To clarify the variability of the limit state exceedance probability within the investigated number of simulations, the COV was calculated by using the following equation:

$$\text{COV}_k^{P_i} = \frac{\sigma_k^{P_i}}{\mu_k^{P_i}} \quad (24)$$

where $\text{COV}_k^{P_i}$ is the COV of the limit state exceedance probability over a specified range of the number of simulations k . $\mu_k^{P_i}$ and $\sigma_k^{P_i}$ are the average and standard deviation of the limit state exceedance probability, respectively, obtained from the following equations:

$$\mu_k^{P_i} = \frac{1}{NS} \sum_{i=k-NS+1}^k P_{l,i}$$

$$\sigma_k^{P_i} = \sqrt{\frac{\sum_{i=k-NS+1}^k (P_{l,i})^2 - NS \cdot (\mu_k^{P_i})^2}{NS - 1}} \quad (25)$$

where NS is the investigated number of simulations. Generally, the required number of simulations to calculate the average and standard deviation of the limit state exceedance probability should be greater than its inverse.

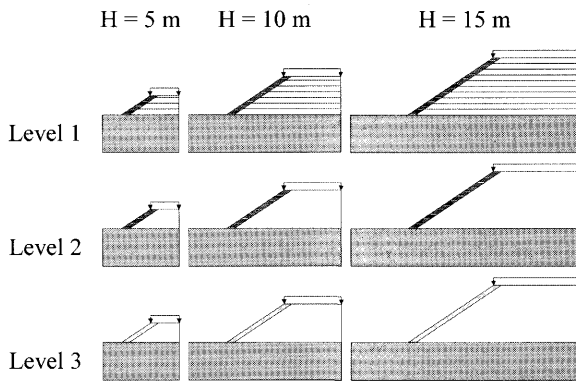


Fig. 6. Analytical models of the typical earth slopes and GRS slopes

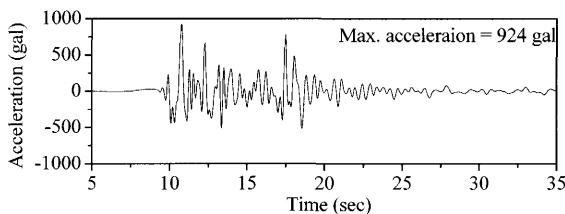


Fig. 7. A standard design ground motion employed in the Newmark analysis for the seismic design of railway earth slopes and GRS slopes in Japan

Table 2. Reinforcement properties

Category	Warranted tensile strength specified by a manufacturer	
	Average (kN/m)	COV
Primary reinforcement	30	10%
Secondary reinforcement	2	10%

Table 1. Classification of the properties of backfill and surface soils

Group	Unit weight		Friction angle			Cohesion		
	Average (kN/m ³)	COV	Average (degrees)		COV	Average (kN/m ²)		COV
			Backfill	Surface		Backfill	Surface	
A	20	5%	45	40	10%	6	3	10%
B	19	5%	40	35	10%	6	3	10%
C	18	5%	35	30	10%	6	3	10%

On the basis of the trial simulation results in this analysis, for the CMC and LDSMC methods, NS was set as the inverse of the limit state exceedance probability multiplied by 100. For the ISLDSMC method, NS was set constant at 100.

The effect of the number of simulations over the specified range of low to high limit state exceedance probabilities was investigated. Two types of analytical models were used as representatives with a low or high limit state exceedance probability. One model had a constant slope height of 10 m and the properties of the backfill soil corresponded to group C, as listed in Table 1; this was expected with a high limit state exceedance probability. The other had a constant slope height of 10 m, and the properties of the backfill soil corresponded to group B, as listed in Table 1; this was expected with a low limit state exceedance probability. The geometries of the both the models were set at structural level 1, as shown in Fig. 5.

Deterministic and Probabilistic Seismic Deformation Analyses

In order to investigate the effects of soil properties, slope heights, and structural levels on the seismic deformation or limit state exceedance probability, the deterministic and probabilistic seismic deformation analyses were conducted with the Newmark analysis. First, the location of the center and radius of the critical slip surface at the yield acceleration was investigated by the deterministic Newmark analysis. In this analysis, a basic model with a constant slope height of 5 m, properties of the backfill soil corresponding to group A (Table 1), and geometry of structural level 1 (Fig. 5) was analyzed. Then, the location of the critical slip surface was investigated by changing the slope height (10 m or 15 m), backfill soil properties (group B or C), and structural level (2 or 3), respectively. Next, the nomograms on the seismic deformation and limit state exceedance probability were obtained. The limit state exceedance probability was calculated on the basis of the performance function expressed in Eq. (19), using the critical seismic deformation of 50 cm for the seismic deformation. As shown in Fig. 6, the slope heights were 5, 10, and 15 m; the soil properties were groups A, B, and C; and the geometries of the models corresponded to structural levels 1, 2, and 3. On the other hand, the average values of the soil properties were used for the deterministic analysis. In the present study, the fixed design ground motion was assigned to both the deterministic and probabilistic Newmark analyses.

RESULTS

Verification of Proposed Quasi-Monte Carlo Method

The biases of CMC, LDSMC, and ISLDSMC simulations for the high limit state exceedance probability are shown in Fig. 8(a). The results using the CMC method were relatively unstable even for a large number of simulations. By the CMC method, when the number of simulations was 5000, a limit state exceedance probability of

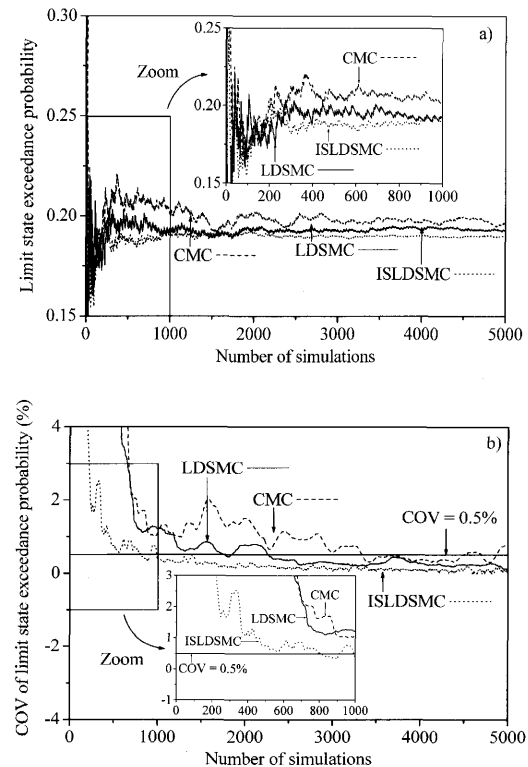


Fig. 8. Bias of crude Monte Carlo (CMC) simulation, low-discrepancy sequence Monte Carlo (LDSMC), and importance sampling with low-discrepancy sequence Monte Carlo (ISLDSMC) simulations with the number of simulations ranging up to 5000 for the high limit state exceedance probability calculation: a) Limit state exceedance probability and b) COV of the limit state exceedance probability

0.196 was obtained in which the corresponding reliability index obtained from Eq. (21) is 0.855. Figure 8(b) shows the COV of the limit state exceedance probability obtained from Eq. (24) versus the number of simulations. The investigated number of simulations (NS) in Eq. (25) was set as 500. The general trend is that the COV decreased with an increase in the number of simulations. Over a particular range of the number of simulations investigated, the COVs of the limit state exceedance probability by the CMC method were relatively unstable and greater than the results from the other methods. The above results indicate that a large number of simulations is required to obtain the convergence of the limit state exceedance probability and to reduce its variance with the CMC method. On the other hand, the limit state exceedance probabilities by the LDSMC and ISLDSMC methods showed a more stable behavior. The results of the LDSMC and ISLDSMC methods revealed almost the same limit state exceedance probabilities with an increase in the number of simulations, while a discrepancy exists between these results under a small number of simulations. The COVs of the limit state exceedance probability by the LDSMC and ISLDSMC methods exhibited lower values than those by the CMC method. The above trend was slightly pronounced with the ISLDSMC method. These results indicate that, due to the uniformity in the input parameters, the LDSMC and ISLDSMC simula-

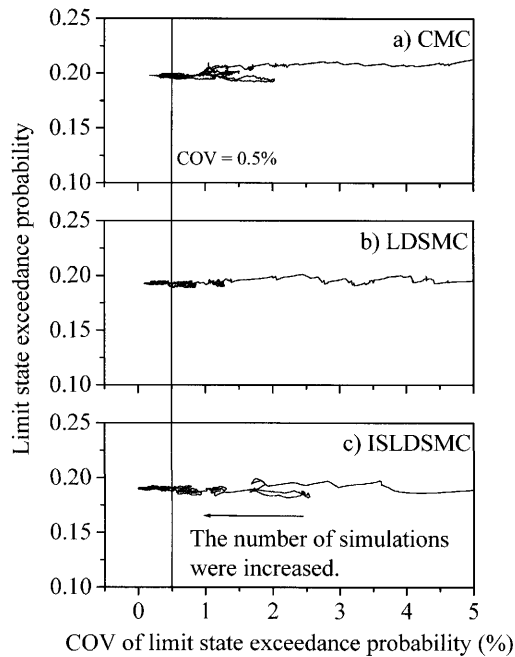


Fig. 9. Convergence of the Monte Carlo simulation with regard to the COV of the limit state exceedance probability for the high limit state exceedance probability calculation: a) CMC simulation, b) LDSMC simulation and c) ISLDSMC simulation

tions are stable and easy to converge, resulting in calculations that are less time-consuming.

The limit state exceedance probabilities by the CMC, LDSMC, and ISLDSMC methods are plotted against the corresponding COVs, as shown in Fig. 9. It is clearly observed that the limit state exceedance probabilities tend to converge with a decrease in the COVs. This trend was more pronounced with the LDSMC and ISLDSMC methods. These results indicate that it is fairly reasonable to infer that the convergence of the Monte Carlo simulation was determined by the specific COV of the limit state exceedance probability. This issue will be explained later.

Figure 10(a) shows the biases of the CMC, LDSMC, and ISLDSMC simulations for the low limit state exceedance probability. The limit state exceedance probability by the CMC method was unstable and unlikely to converge when the number of simulations reached 60,000. As shown in Fig. 10(b), the COV of the limit state exceedance probability with the investigated number (NS) of 3000 in Eq. (25) was greater than those by the LDSMC and ISLDSMC methods, especially at the beginning of the simulation. As a result, a limit state exceedance probability of 0.0356 (the corresponding reliability index is 1.804) was obtained by the CMC method when the number of simulations was 80,000. On the other hand, the limit state exceedance probability by the LDSMC method converged with a lower number of simulations as compared to the CMC simulation. Moreover, the COV of the limit state exceedance probability by the LDSMC method exhibited a lower value than that by the CMC method. Consequently, a limit state exceedance probability of 0.0362 (the corre-

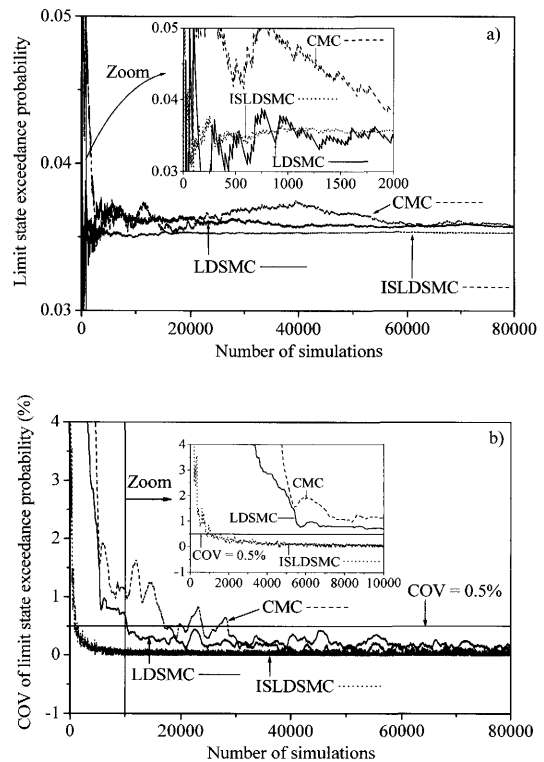


Fig. 10. Bias of CMC, LDSMC, and ISLDSMC simulations with the number of simulations ranging up to 5000 for the low limit state exceedance probability calculation: a) Limit state exceedance probability and b) COV of limit state exceedance probability

sponding reliability index is 1.797) was obtained by the LDS method when the number of simulations reached 10,000; this result is practically the same as that by the CMC method even at lower number of simulations. However, even when the LDSMC method is applied for calculating the limit state exceedance probability, it is not practically useful due to its longer computation time for the calculation of the lower limit state exceedance probability. The most effective method for this calculation is to employ the ISLDSMC method. It is clearly observed in Fig. 10 that a limit state exceedance probability of 0.0359 (the corresponding reliability index is 1.800) was obtained when the number of simulations was 1000; this result is practically the same as those by the CMC and LDSMC method when the number of simulations was 80,000. If the conventional stability analysis takes 0.1 sec approximately, the computational time of the CMC method and ISLDSMC method were 2:13:20 (hour:min:sec) and 1:40 (min:sec) based on the above numerical conditions. Furthermore, the COV of the limit state exceedance probability by the ISLDSMC method showed a considerably lower value than the others even when the number of simulations was 500. These results demonstrate that the ISLDSMC method is optimum for the lower limit state exceedance probability calculation. Figure 11 shows the limit state exceedance probability plotted versus its COV for all the methods. Trends similar to those observed in Fig. 9 were observed. Based on the above comparison, it is quite reasonable to use the

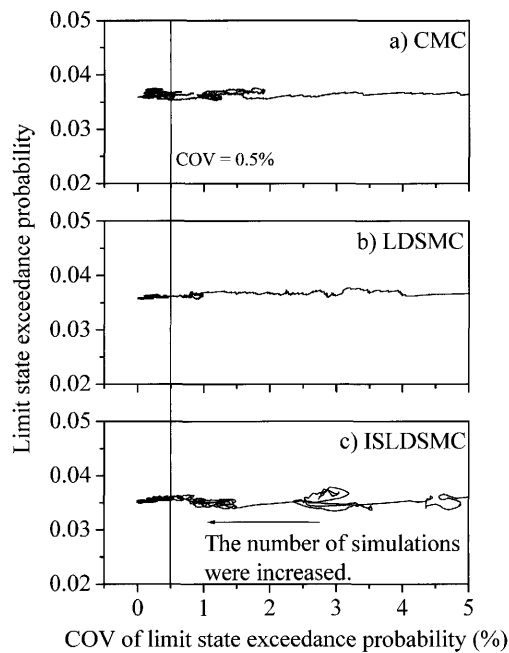


Fig. 11. Convergence of the Monte Carlo simulation with regard to the COV of the limit state exceedance probability for the low limit state exceedance probability calculation: a) CMC simulation, b) LDSMC simulation and c) ISLDSMC simulation

proposed LDSMC and ISLDSMC methods for the low to high limit state exceedance probability calculations.

In summary, the computational efficiency between the LDSMC and ISLDSMC methods was almost identical for the high limit state exceedance probability calculation, while the ISLDSMC method was the most effective for the low limit state exceedance probability calculation. However, in the ISLDSMC method, a failure region should be expected by the FORM, as mentioned above. This indicates that the LDSMC method is simpler than the ISLDSMC method. Therefore, in the current analysis, the LDSMC or ISLDSMC method was used to evaluate the limit state exceedance probability greater than 0.1 or less than 0.1, respectively.

The Monte Carlo simulation is generally conducted until the prescribed number of simulations. This is based on the fact that the accuracy of a simulation result improves with an increase in the number of simulations. However, there still exists a possibility that an unstable simulation result is achieved unless the number of simulations is sufficiently high. Therefore, in this study, the convergence of the Monte Carlo simulation was determined by the specific COV of the limit state exceedance probability. Figures 9 and 11 show that the limit state exceedance probability by the LDSMC and ISLDSMC methods reasonably converged with the values of the COV of the limit state exceedance probability lower than 0.5%. It is important for engineers to note that the required accuracy of the solution and tolerance of the COV should be determined by considering the computation time. In practice, if the required accuracy is important, a long time would be required to obtain the

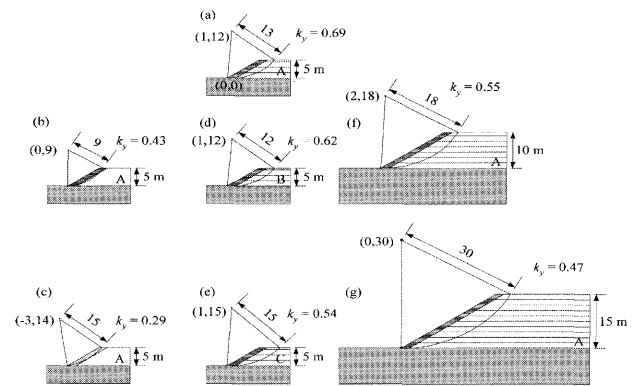


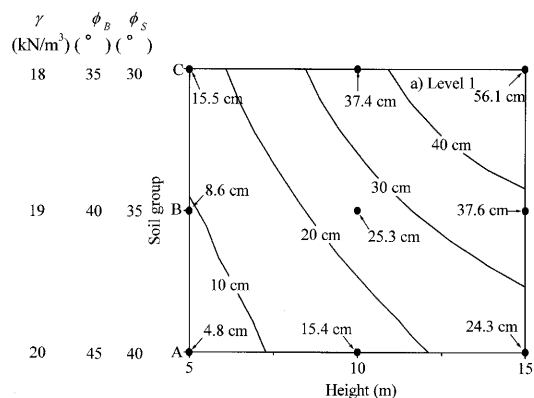
Fig. 12. Critical circular slip surface with variable structural levels, soil properties, and slope heights: a) Structural level 1, soil group A, and slope height of 5 m, b) Structural level 2, soil group A, and slope height of 5 m, c) Structural level 3, soil group A, and slope height of 5 m, d) Structural level 1, soil group B, and slope height of 5 m, e) Structural level 1, soil group C, and slope height of 5 m, f) Structural level 1, soil group A, and slope height of 10 m and g) Structural level 1, soil group A, and slope height of 15 m

solution. In this paper, referring to Figs. 9 and 11, the tolerance of the COV is precisely set at 0.5% in the following simulations.

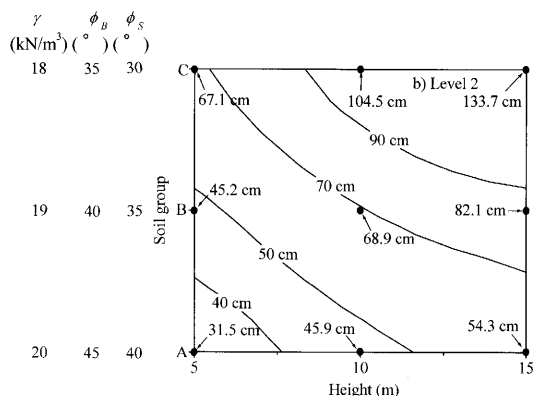
Deterministic Seismic Deformation Analysis Results

For the adopted simplified Newmark analysis, the seismic stability analysis was conducted to obtain the center and radius of the critical circular slip surface at a yield acceleration that strongly affects the seismic deformation. Figure 12 shows the critical slip surface and yield acceleration obtained from Eq. (2) in each case. Figures 12(a), 12(b), and 12(c) show the effect of structural level on the critical slip surface; the soil properties and slope heights were identical in these figures. For structural level 1 (Fig. 12(a)), the critical slip surface at a high yield acceleration was located beyond the secondary reinforcement, while shallow slip surfaces were obtained for structural levels 2 and 3 at lower yield accelerations (Figs. 12(b) and 12(c)). These results indicate that yield acceleration strongly depends on the structural level, and reinforcement can contribute to increase seismic stability. Figures 12(a), 12(d), and 12(e) show the effect of backfill soil properties on the critical slip surface; the slope heights and structural levels were identical in these figures. The critical slip surfaces were practically the same even when changing the backfill soil properties. However, the yield acceleration was sensitive to the backfill soil properties. The slope height had a small effect on the critical slip surface, as shown in Figs. 12(a), 12(f), and 12(g), while the yield acceleration decreased with an increase in the slope height.

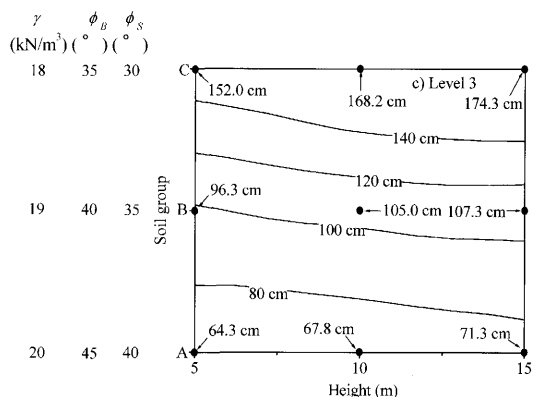
Figure 13 shows the nomogram of seismic deformation obtained by changing the soil properties and slope heights for a constant structural level. Since the soil group is primarily not a continuous variable, such a nomogram of the seismic deformation may not be appropriate. However, the soil properties, for example, density or fric-



(a)



(b)



(c)

Fig. 13. Nomogram of seismic deformation on earth slopes and GRS slopes with a constant structural level but variable soil properties and slope height by the deterministic Newmark analysis: a) Level 1, b) Level 2 and c) Level 3

tion angle, in each soil group is a continuous variable, as shown in Table 1. Therefore, in this study, it is considered that it would be practically useful to show such nomograms of seismic deformation obtained by varying the soil properties and slope heights. The soil properties of each soil group and the original data were superimposed to create the nomogram, as shown in the figures. Based on these nomograms, the sensitivity of the seismic deformation is evaluated in this study under the specified

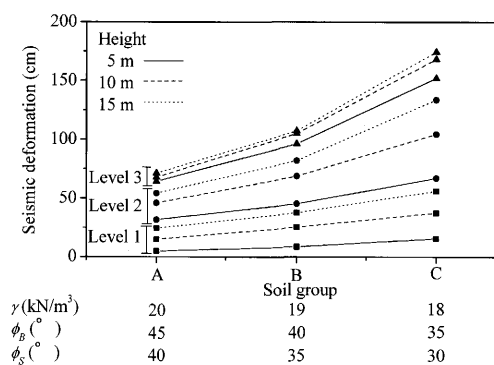


Fig. 14. Influence of soil properties, slope height, and structural level on the seismic deformation of the earth slopes and GRS slopes by the deterministic Newmark analysis

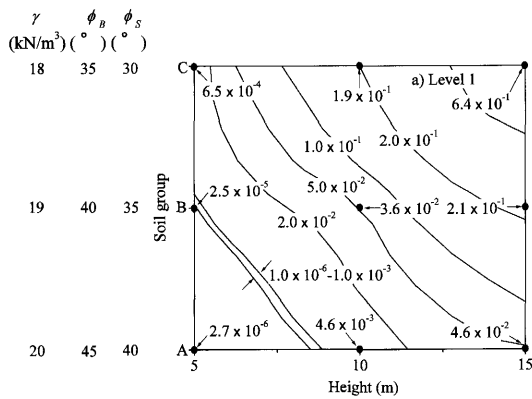
range of the soil properties and slope heights described in Fig. 13. For structural level 1, the seismic deformation had a higher sensitivity to the slope height than the soil properties. For structural level 2, the sensitivities of the slope height and soil properties were similar to each other. For structural level 3, the seismic deformation had a lower sensitivity than the slope height, while the seismic deformation had a considerably higher sensitivity than the soil properties.

Figure 14 shows the seismic deformation plotted against the soil group in each structural level for a constant slope height. Generally, the seismic deformation increased with the degradation of the structural level and soil properties. More specifically, the seismic deformation was sensitive to the structural level in all the cases, while it was also sensitive to the soil properties for the lower structural levels; this was in accordance with the results shown in Fig. 13.

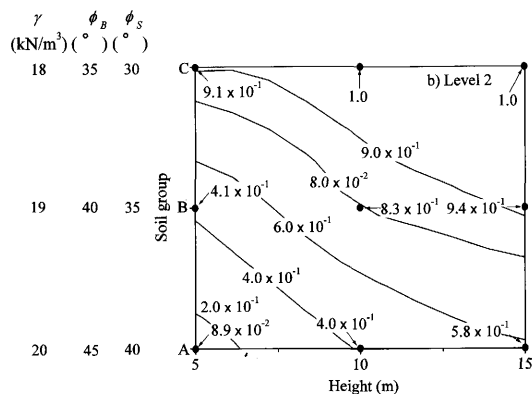
Probabilistic Seismic Deformation Analysis Results

Figure 15 shows the nomogram of the limit state exceedance probability under the same numerical conditions as used for Fig. 13, except that the statistical data is considered (i.e., COVs of the soil properties and the design strength of reinforcement). Generally, the limit state exceedance probability of the earth slopes or GRS slopes for a critical seismic deformation of 50 cm increased with the slope height, degrading the properties of the backfill soil or structural level; this was consistent with the results obtained from the deterministic Newmark analysis. More specifically, in Fig. 15(a), the limit state exceedance probability of the GRS slope with the properties of the backfill soil corresponding to group A, slope height of 5 m, and structural level 1 exhibited a low value, which was less than 1.0×10^{-5} such that the reliability of the GRS slope was considerably higher than that of any other slopes. Meanwhile, the earth slopes and GRS slopes with structural levels 2 and 3, respectively, had relatively high limit state exceedance probabilities that scarcely exceeded 1.0×10^{-1} even with the properties of the backfill soil corresponding to group A.

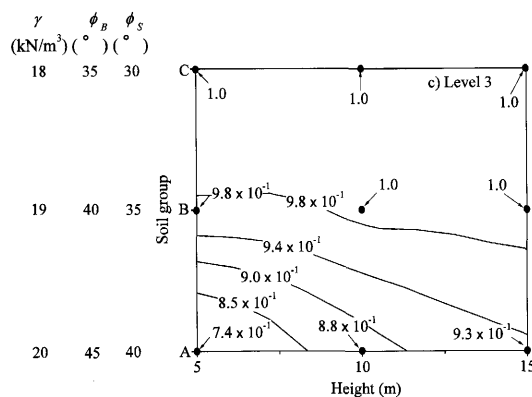
Figure 16 shows the limit state exceedance probability



(a)



(b)



(c)

Fig. 15. Nomogram of limit state exceedance probability on the earth slopes and GRS slopes with a constant structural level but variable soil properties and slope height by the probabilistic Newmark analysis: a) Level 1, b) Level 2 and c) Level 3

plotted against the soil group in each structural level for a constant slope height. Generally, the limit state exceedance probability increased with the degradation of the structural level and soil properties. More specifically, the limit state exceedance probability was sensitive to the structural level in all the cases, while it was also sensitive to the soil properties for the structural level 2.

The allowable limit state exceedance probability should be determined by engineers or constructors before

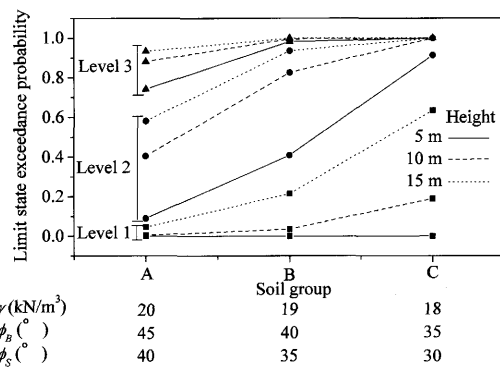


Fig. 16. Influence of soil properties, slope height, and structural level on the seismic deformation of earth slopes and GRS slopes by the deterministic Newmark analysis

designing. For temporal structures, the limit state exceedance probability may be set higher due to their shorter lifetime, while for important permanent structures, a lower limit state exceedance probability should be set. For the latter case, under the conditions employed in the present study, the primary and secondary reinforcements should be installed (i.e., structural level 1 should be attained); the design strength of the primary reinforcement should be high enough; and high-quality soil (group A) should be used. The required design strengths of the reinforcements to satisfy the prescribed reliability of structures will be reported elsewhere in the near future.

DISCUSSION

For quick, accurate, and practically useful limit state exceedance probability calculations, it is important to recognize the relationship between the critical seismic deformation obtained from the deterministic Newmark analysis and the limit state exceedance probability under this deformation. Figure 17 shows the limit state exceedance probability under the specific critical seismic deformation of 50 cm plotted versus the seismic deformation obtained by varying the soil properties and structural level for a constant slope height. Generally, both the limit state exceedance probability and seismic deformation were most sensitive to the structural level. The earth slopes and GRS slopes showing a seismic deformation of around 50 cm or more obtained from the deterministic Newmark analysis exhibited high limit state exceedance probabilities exceeding 0.5. These results show that the seismic deformation of reliable earth slopes and GRS slopes should not exceed the specific critical seismic deformation (50 cm in the present study). Figure 17 also indicates that, for example, if the allowable limit state exceedance probability is 0.01, the corresponding amount of seismic deformation obtained from the deterministic Newmark analysis should be less than 25 cm under the assumed input parameters used in this study.

Figure 18 shows a typical histogram of the seismic deformation with a constant slope height of 10 m, properties of the backfill soil corresponding to group A

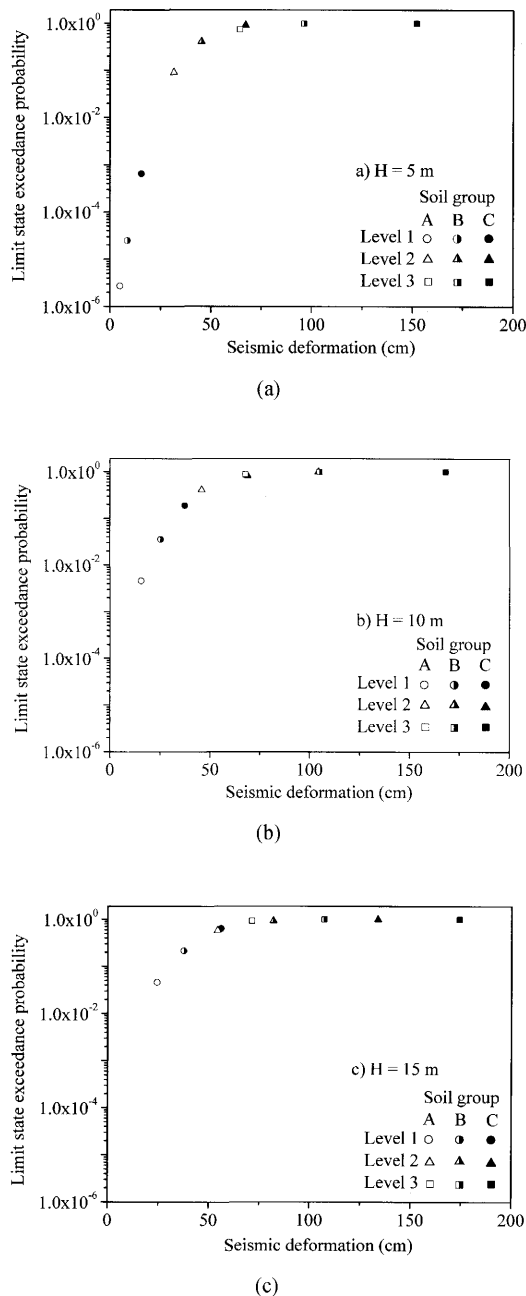


Fig. 17. Relationship between the limit state exceedance probability and seismic deformation of earth slopes and GRS slopes with a constant slope height but variable soil properties and structural level: a) 5 m in height, b) 10 m in height and c) 15 m in height

(Table 1), and geometry of structural level 1 obtained from the LDSMC method. The statistical data obtained from the LDSMC, an approximated statistical distribution for the histogram, and the seismic deformation obtained from the deterministic Newmark analysis were superimposed on this figure. Importantly, it is clearly observed that the statistical distribution of seismic deformation could be approximated to be a log normal distribution with an average value (μ_x) of 39.6 cm, standard deviation (σ_x) of 14.0 cm, and COV of 0.354 obtained from the LDSMC simulation. To calculate the limit state exceedance probability from the estimated log

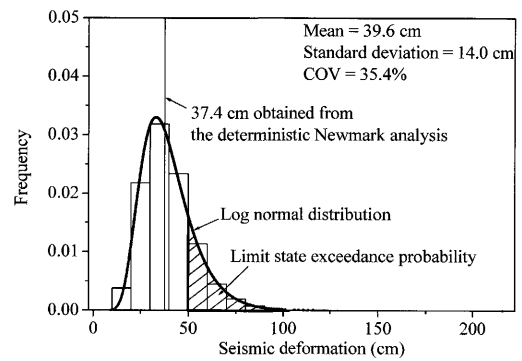


Fig. 18. Histogram of the seismic deformation of a GRS slope with a constant slope height of 10 m, soil group A, and structural level 1 by the LDSMC method

normal distribution, the area of the tail exceeding the critical seismic deformation (50 cm in the present study) was obtained from the following equation:

$$P_1 = \int_{D_L}^{\infty} f(x) dx \quad (26)$$

where P_1 is the limit state exceedance probability; D_L , critical seismic deformation; and $f(x)$, log normal probability density function defined as

$$f(x) = \frac{1}{\sqrt{2\pi} \cdot \zeta \cdot x} \exp \left[-\frac{1}{2} \left(\frac{\ln x - \lambda}{\zeta} \right)^2 \right] \quad (0 < x < \infty) \quad (27)$$

where λ is the average of $\ln x$, and ζ is the standard deviation of $\ln x$. More specifically, λ and ζ can be calculated as follows:

$$\lambda = \ln \mu_x - \frac{1}{2} \zeta^2 \quad (28)$$

$$\zeta = \sqrt{\ln \left(1 + \frac{\sigma_x^2}{\mu_x^2} \right)} = \sqrt{\ln (1 + \text{COV}^2)} \quad (29)$$

The limit state exceedance probability by the LDSMC method was 0.189, while the estimated limit state exceedance probability obtained from the assumed log normal distribution using the average of 39.6 and COV of 0.354 was 0.198. There is a slight discrepancy due to the approximation; however, it is considered that in practice, this discrepancy would be negligible. The above comparison indicates that it may be possible to estimate the limit state exceedance probability using the approximated log normal probability density function.

According to the above approximation, the average and standard deviation should be determined to initially estimate the limit state exceedance probability. Based on the trial simulation results, in the present study, the average of the seismic deformation was set as the seismic deformation obtained from the deterministic Newmark analysis, and the COV of the seismic deformation was assumed at a constant value of 0.5.

Figure 19 shows the comparison between the estimated limit state exceedance probabilities by the above approximation and those by the Monte Carlo simulation in all

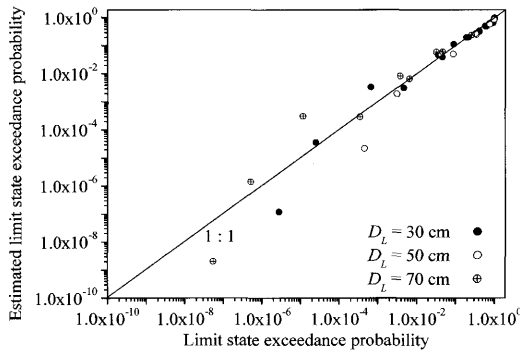


Fig. 19. Verification of the estimated limit state exceedance probability with that by the LDSMC method

the cases adopted in this study ($D_L = 50$ cm) and additional cases with the same numerical condition, except for structural level 1 and different critical seismic deformations ($D_L = 30$ cm and $D_L = 70$ cm). Generally, the estimated limit state exceedance probability is in good agreement with the simulation results over a wide range of limit state exceedance probabilities. When observed in detail, a discrepancy exists with regard to low limit state exceedance probabilities (less than 1.0×10^{-3}). This discrepancy is mainly due to the use of the approximation for statistical distribution, where the average is identical to the seismic deformation obtained from the deterministic Newmark analysis and the prescribed COV of the seismic deformation. In practice, a simple estimation of the limit state exceedance probability would be preferred. Careful attention would be required while using the above approximation for estimating lower limit state exceedance probabilities.

CONCLUSIONS

The paper reports an explicit technique to compute the limit state exceedance probability of earth slopes (without reinforcement) and geosynthetic-reinforced soil (GRS) slopes using a low-discrepancy sequence Monte Carlo (LDSMC) method and an importance sampling with low-discrepancy sequence Monte Carlo (ISLDSMC) method with the Newmark's sliding block analysis (Newmark analysis). These techniques have an advantage over the conventionally used crude Monte Carlo (CMC) simulation that becomes unstable under a small number of simulations, thereby inducing impermissible numerical error. The LDSMC method is applicable for the calculation of high limit state exceedance probabilities, while the ISLDSMC method enables accurate calculation over a wide range of limit state exceedance probabilities under a significantly small number of simulations.

The numerical results presented in this paper reveal that the seismic deformation and limit state exceedance probability of earth slopes or GRS slopes increased with the slope height and degradation of the backfill soil properties or structural level. The seismic deformation and its limit state exceedance probability were the most sensitive

to the structural level. Finally, in order to increase the seismic stability of earth slopes with regard to the limit state exceedance probability, primary and secondary reinforcement should be installed and high-quality backfill soil should be used, especially in higher GRS slopes.

In order to make limit state exceedance probabilities practically useful, a simple approximation to estimate it by using the average that is identical to the seismic deformation obtained from the deterministic Newmark analysis and the prescribed COV of the seismic deformation was proposed. The estimated limit state exceedance probability is in good agreement with that obtained from the LDSMC simulation, except for the cases with low limit state exceedance probabilities. Therefore, the proposed approximation should be used by carefully considering the available order (1.0×10^{-3} to 1.0 in the present study) of the limit state exceedance probability.

Additional research is required to investigate the effect of foundation soil properties, slope inclination, embedment length and vertical spacing of the reinforcement, and, in particular, the spatial variability of backfill soil, foundation soil, and reinforcement on the evaluation of limit state exceedance probability. The economic cost-benefit evaluation with life-cycle cost obtained from the current limit state exceedance probability will be reported elsewhere in the near future, considering the occurrence rate of different levels of seismic motions.

REFERENCES

- Alonso, E. E. (1976): Risk analysis of slope and its application to slopes in Canadian sensitive clays, *Geotechnique*, **26**(3), 453–472.
- Bergado, D. T. and Anderson, L. R. (1985): Stochastic analysis of pore pressure uncertainty for the probabilistic assessment of the safety of earth slopes, *Soils and Foundations*, **25**(2), 87–105.
- Bernardi, M. and Paulson, J. (1997): Is creep a degradation phenomenon? *Mechanically Stabilized Backfill* (ed. by Wu, J. T. H.), Balkema, 289–294.
- Box, G. E. P. and Muller, M. E. (1958): A note on the generation of random normal deviates, *Ann. Math. Stat.*, **29**, 610–611.
- Chalermyanont, T. and Benson, C. H. (2004): Reliability-based design for internal stability of mechanically stabilized earth walls, *J. Geotech. Geoenviron. Engrg.*, **130**(2), 163–173.
- Christian, J. T., Ladd, C. C. and Baecher, G. B. (1994): Reliability applied to slope stability analysis, *J. Geotech. Engrg.*, **120**(12), 2180–2207.
- Duncan, M. J. (2000): Factors of safety and reliability in geotechnical engineering, *J. Geotech. Geoenviron. Engrg.*, **126**(4), 307–593.
- El-Ramly, H., Morgenstern, N. R. and Cruden, D. M. (2002): Probabilistic slope stability analysis for practice, *Can. Geotech. J.*, **39**, 665–683.
- Fellenius, W. (1927): *Erdstatische Berechnungen mit Reibung und Kohäsion (Adhäsion) und unter Annahme kreiszylindrischer Gleitflächen*, W. Ernst und Sohn Verlag, Berlin.
- Greenwood, J. H. (1997): Designing to residual strength of geosynthetics instead of stress-rupture, *Geosynth. Int.*, **4**(1), 1–10.
- Greenwood, J. H., Kempton, G. T., Watts, G. R. A. and Bush, D. I. (2000): Twelve year creep tests on geosynthetic reinforcements, *Proc. EuroGeo 2000*, 333–336.
- Greenwood, J. H., Jones, C. J. F. P. and Tatsuoka, F. (2001): Residual strength and its application to design of reinforced soil in seismic areas, *Proc. Int. Symp. Earth Reinforcement* (eds. by Ochial et al.), Balkema, **1**, 37–42.
- Hasofer, A. M. and Lind, N. C. (1974): Exact and invariant second-moment code format, *J. Engrg. Mech. Div.*, **100**(1),

- 111–121.
- 14) Hoeg, K. A. M. and Murarka, R. P. (1974): Probabilistic analysis and design of a retaining wall, *J. Geotech. Engrg.*, **100**(3), 349–365.
 - 15) Li, K. S. and Lumb, P. (1987): Probabilistic design of slopes, *Can. Geotech. J.*, **24**(4), 520–535.
 - 16) Lian, Y. and Yen, B. C. (2003): Comparison of risk calculation methods for a culvert, *J. Hydraulic Engineering*, **129**(2), 140–152.
 - 17) Low, B. K. and Tang, W. H. (1997): Reliability analysis of reinforced embankment on soft ground, *Can. Geotech. J.*, **34**(5), 672–685.
 - 18) Matsuo, M. and Kuroda, K. (1974): Probability approach to design of embankments, *Soils and Foundations*, **14**(2), 1–17.
 - 19) Newmark, N. M. (1965): Effects of earthquakes on dams and embankment, *Geotechnique*, **15**(2), 139–160.
 - 20) Orsat, P., Khay, M. and McCreath, M. (1998): Study on creep-rupture of polyester tendons: full scale tests, *Proc. 6th Int. Conf. Geosynth.*, **2**, 675–678.
 - 21) Railway Technical Research Institute (RTRI) (2000): *Design Standard for Railway Earth Structures*, Railway Technical Research Institute, Maruzen (in Japanese).
 - 22) Ribenboim, P. (1996): *The New Book of Prime Number Records*, New York, Springer-Verlag, 22–25.
 - 23) Shinoda, M., Bathurst, R. J., Tatsuoaka, F. and Horii, K. (2002): Time dependent deformation and strength characteristics of viscous geogrids, *J. Geosynth.*, **17**, 137–144 (in Japanese).
 - 24) Shinoda, M., Yonezawa, T., Tateyama, M. and Koseki, J. (2005): Limit state exceedance probability of reinforced soil retaining walls, *J. Jpn. Soc. Civil Engineers*, (792/III-71), 119–129 (in Japanese).
 - 25) Tamura, T. and Shirakawa, H. (1999): Quasi random number by the generalized Faure sequence and its application to the option evaluation, *JAFEE J.*, 95–111 (in Japanese).
 - 26) Tang, W. H., Yucemen, M. S. and Ang, A. H.-S. (1976): Probability-based short term design of soil slopes, *Can. Geotech. J.*, **13**, 201–215.
 - 27) Tezuka, S. (1995): *Uniform Random Numbers: Theory and Practice*, Kluwer Academic Publishers, Boston.
 - 28) Vanmarcke, E. H. (1977): Reliability of earth slopes, *J. Geotech. Engrg.*, **103**(11), 1247–1265.
 - 29) Voskamp, W., Vliet, F. and Retzlaff, J. (2001): Residual strength of PET after more than 12 years creep loading, *Proc. Int. Symp. Earth Reinforcement* (eds. by Ochiai et al.), Balkema, **1**, 165–170.
 - 30) Watanabe, K., Ohki, M., Shinoda, M., Kojima, K. and Tateyama, M. (2005): A series of triaxial compression tests on strength of soil material for stability analysis of embankment, *RTRI Report*, **19**(3), 29–34 (in Japanese).
 - 31) Wu, T. H. and Kraft, L. M. (1970): Safety analysis of slopes, *J. Soil Mech. Found. Div.*, **96**(2), 609–630.

APPENDIX: LOW-DISCREPANCY SEQUENCE

According to reference literature (Tamura and Shirakawa, 1999), the generalized Faure sequence $X_n = (X_n^{(1)}, X_n^{(2)}, \dots, X_n^{(k)})$ with a dimension of k (k is equal to 8 in this study) is defined as follows:

$$X_n^{(i)} = \frac{a_0^{(i)}}{b} + \frac{a_1^{(i)}}{b^2} + \dots + \frac{a_r^{(i)}}{b^{r+1}} \quad (\text{A1})$$

where i is the dimension of the random variables; b , the cardinal number and minimum prime number greater than dimension k (for example, if $k=8$ then $b=11$); r , the number of the term including b of the base- b digits of the number of random variables in each dimension n ; and a , the coefficient given by

$$\begin{pmatrix} a_0^{(1)} \\ a_1^{(1)} \\ \vdots \\ a_r^{(1)} \end{pmatrix} = \begin{pmatrix} p & & \\ & p & \\ & & p \end{pmatrix} \cdot \begin{pmatrix} a_0 \\ a_1 \\ \vdots \\ a_r \end{pmatrix} \quad (i=1) \quad (\text{A2})$$

$$\begin{pmatrix} a_0^{(i)} \\ a_1^{(i)} \\ \vdots \\ a_r^{(i)} \end{pmatrix} = \begin{pmatrix} p_i & & \\ & p_i & \\ & & p_i \end{pmatrix} \cdot \begin{pmatrix} {}_0C_0 & {}_1C_0 & {}_2C_0 & \dots \\ & {}_1C_1 & {}_2C_1 & \dots \\ & & {}_2C_2 & \dots \\ & & & \ddots \end{pmatrix}^{i-1} \times \begin{pmatrix} a_0 \\ a_1 \\ \vdots \\ a_r \end{pmatrix} + \delta \begin{pmatrix} i \\ i \\ \vdots \\ i \end{pmatrix} \pmod{b} \quad (i \geq 2) \quad (\text{A3})$$

where p and p_i are obtained from the following equations:

$$p = p_1 \quad (\text{A4})$$

$$p_i = q^i \pmod{b} \quad (\text{A5})$$

where q is the minimum primitive root such that $q \pmod{b}$ has modulo order $b-1$ (Ribenboim, 1996). For example, the minimum primitive root of $b (=11$ in this study) is the integer 2. Tamura and Shirakawa (1999) employed $\delta=1.0$ in Eq. (A3). However, in this study, $\delta=0.0$ was used for the purpose of simplicity. ${}_sC_t$ is the binomial coefficient expressed as follows:

$${}_sC_t = \frac{s!}{(s-t)!t!} \quad (\text{A6})$$

$(a_0 \ a_1 \ \dots \ a_r)'$ in Eq. (A2) and Eq. (A3) is the following coefficient of the base- b digits of the number of random variables in each dimension n .

$$n = a_0 + a_1b + \dots + a_rb^r \quad (\text{A7})$$